Desalination and Water Treatment
www.deswater.com

doi:10.5004/dwt.2019.23441

141 (2019) 321–330
February

Synthesis of CuS/graphene porous composite for adsorption synergistic photocatalytic degradation of methyl orange

Tingwei Cai, Ying Ding*, Lihui Xu

College of Fashion and Textile, Shanghai University of Engineering Science, Shanghai 201620, China, email: tingvcai@163.com (T. Cai), tingying@sues.edu.cn (Y. Ding), xulh0915@163.com (L. Xu)

Received 27 June 2018; Accepted 6 November 2018

ABSTRACT

Three-dimensional porous CuS/graphene photocatalysts had been successfully prepared by two-step solvothermal method and exhibited outstanding adsorption synergistic photodegradation for anion dyemethyl orange (MO). Due to the combination of the adsorption of graphene porous aerogel and the photocatalysis of CuS, the CuS/graphene photocatalysts could rapidly enrich the methyl orange and effectively degrade MO in suit. The degradation rate of MO went up to as high as 92.94% by the CuS/graphene composites in 55 min through the synergistic effect of adsorption photocatalytic, which was about 2.9 times more than that of bare CuS. The obviously improved photodegradation rate was attributed to the excellent adsorption performance and high charge mobility of the porous graphene substrate. Moreover, its MO removal efficiency still remained 79.47% after 3 times cyclic experiments. Meanwhile, due to its special 3D porous network structure, the CuS/graphene composites could efficiently separate from the solution without assistance of filtering. Therefore, the CuS/graphene composites with the synergy of adsorption and photocatalysis would be a promising strategy for practical dye wastewater treatment.

Keyword: CuS/graphene hydrogel; CuS; synergy of adsorption and photocatalysis; 3D porous structure; MO removal

1. Introduction

Nowadays, the growing development of industry have caused more and more serious water pollution. For instance, dyestuff wastewater is often released into environment without advance treatment. For dyestuff wastewater, the familiar treatment methods are adsorption [1]. The adsorbents with a high surface area and optimal pore structure have excellent adsorption capacity, but they have the shortcomings of difficult to desorption and regeneration, poor selectivity, secondary pollution and other issues [2,3]. Therefore, there is an urgent need to develop a new method to remove the dye stuff wastewater.

Photocatalytic technology can effectively use the energy of sunlight to degrade hazardous contaminants in the environment, which has caused widespread concern [4]. The nano-photocatalyst has the characteristics of small size of nanoparticles, incomplete coordination of surface atoms, high photoelectric conversion efficiency and abundant reactive sites, which makes it has excellent photocatalytic activity and efficiency for pollutants [5]. Moreover, nano-photocatalys also has the advantages of complete degradation, no secondary pollution and low cost [6]. However, some shortcomings such as the rapid combination of electron-hole pairs, low visible-light absorption, ease of agglomeration, low adsorption capacity, and difficult recovery limit the practical application of nano-photocatalysts [7]. Therefore, it is necessary to develop a new photocatalyst with high adsorption capacity, outstanding photocatalytic activity and the separation-free feature.

The effective photogenerated electron-hole pairs separation can be attained by construction of catalyst systems via loading nano-photocatalysts into the co-catalyst [8]. Graphene is an ideal substrate for synthesizing

*Corresponding author.

photocatalytic nanocomposites, due to its high electrical conductivity, superior optical performance and large surface area [9]. Therefore, CdS/RGO,g-C_3N_4/rGO, TiO_2/RGO, Ag/AgCl/rGO [8–11] and many other graphene based photocatalysts have been synthesized and applied to degradation of dye wastewater. However, due to the difficulty of separation and recovery from the solution, graphene nano-photocatalysts are hard to industrialize in the near future.

To tackle this problem, porous graphene macrostructures, such as hydrogels and aerogels, have been prepared [10]. The graphene hydrogel (rGH) has better separation performance without complicated filtration systems for recycling. Inheriting all the high electrical conductivity and superior optical performance from the 2D graphene, the 3D graphene network structure also enhances photocatalytic property by enlarging the contact surface area [11]. Besides, the 3D graphene network structure has the following three major advantages that make it the top choice in water purification. First of all, the 3D graphene network, as an electron conductive platform with lower Fermi level, is able to accept and transfer electrons, thus boosting the separation of photogenerated electrons and holes [11,12]. Secondly, these 3D network architectures showed quick mass and electron transport kinetics on account of the large number of irregular cross channels and the excellent inherent photoelectronic property. More than that, the 3D network structure is a good skeleton to load functional nanomaterials, which is able to expose more reactive sites and accelerate the surface photocatalytic reactions [13].

The p-type semiconductor CuS exhibits outstanding photochemical properties because of its narrow band gap of 2.5 eV [14]. Remarkably, CuS exhibits relatively high absorption in the visible and near-infrared region, indicating it is a promising photocatalyst for fully and validly utilizing sunlight energy [15]. However, the photocatalytic activity of CuS is not satisfactory due to the quick recombination of the electron-hole pairs.

In our work, the flower-like CuS photo-catalysts were first uniformly deposited on graphene oxide nanosheets then the 3D porous structural CuS/graphene hydrogel successfully prepared via hydrothermal process. The photocatalytic performance of CuS/graphene hydrogel was evaluated by methyl orange (MO) under Xenon lamp irradiation. The CuS/graphene hydrogels show outstanding synergies of adsorption and photocatalysis for dyes, which is ascribed to the particular porous structure and outstanding electrical conductivity of graphene aerogels. Remarkably, the synergistic effect solves the difficulty of desorption and regeneration of hydrogel and makes it possible to recycle.

2. Materials and methods

2.1. Materials

Thiourea (CH_4N_2S, Tu), Ethylene Glycol ($C_2H_6O_2$, EG), Copper chloride ($CuCl_2{\cdot}2H_2O$) , Methyl Orange (MO) and ethanol were bought from Sinopharm Chemical Reagent Co., Ltd., all of which was analytical reagent and used without further purification. Distilled water was used the whole process.

2.2. Preparation of flower-like CuS

A special synthesis procedure of CuS was conducted as follows: 1.7 g of $CuCl_2{\cdot}2H_2O$ (0.01 mol) was dissolved in 60 mL of EG in a round bottomed flask and then the green transparent solution was heated at 120°C for 20 min under stirring. Then, 3.04 g of CH_4N_2S (0.04 mol) dispersed in 50 mL of ethylene glycol was dripped slowly into the above-mentioned solution within 30 min under stirring. As the mixture became light yellow, it was transformed into 150 mL Teflon-sealed autoclave and maintained at 170°C for 5 h. Finally, the obtained CuS powder was washed and dried.

2.3. Preparation of CuS /graphene hydrogels

GO was prepared from graphite powder employing the Hummer's method [16]. The CuS/graphene porous hydrogels were prepared in the following procedures. 20 mL GO brown colloidal dispersion (6 mg·mL^{-1}) was ultrasonically dispersed in 40 mL of ethanol for 60 min. 0.3 g of CuS and 0.7 g of thiourea were add into 40 mL of ethanol. Then, the mixture of CuS, CH_4N_2S and ethanol was then added into the prepared GO dispersion slowly. After 2 h ofstirring, the homogeneous compound was sealed in 150 ml Teflon-lined autoclave at 180°C for 12 h. After cooling down to the room temperature, the prepared CuS / RGO hydrogel composites sample was immersed in distilled water for 24 h so that the residual thiourea is removed. The two-step synthesis of CuS/RGO hydrogels is illustrated in Fig. 1.

2.4. Photocatalytic performance

The adsorption and photocatalyst properties of different samples were estimated by photodegrading methyl orange (MO, 50 mg·L^{-1}) solution under the Xenon lamp irradiation (200 W). The primary absorption peaks of MO at 464 nm was used as references monitoring the process of catalytic degradation. The MO solution was analyzed by recording the absorbency value at 464 nm using a Hitachi U-3010 UV–vis spectrophotometer. The degradation rate of MO could be calculated by the degradation rate (Dr %):

$$Dr\% = \left(C_0 - C_t\right) / C_0 \times 100\% \tag{1}$$

where C_0 is initial absorbance value of MO solution, C_t is the absorbance of MO at time t under irradiation. Furthermore, photo-catalytic kinetics can be characterized by the Langmuir-Hinshelwood model as:

$$\ln\left(\frac{C_0}{C_t}\right) = k_{obs}\, t \tag{2}$$

where k_{obs} is the reaction rate constant of pseudo-first-order and t is the illumination time.

The experiments were conducted as follows: 0.1 g of bare CuS, 0.1 g and 0.15g of CuS/graphene composites were added into 100 ml of anionic dye-MO (50 mg·L^{-1}) solution, respectively. After a few minutes reaction under Xenon lamp illumination, the absorbance of MO solution measured and recorded using UV-Vis spectrophotometer.

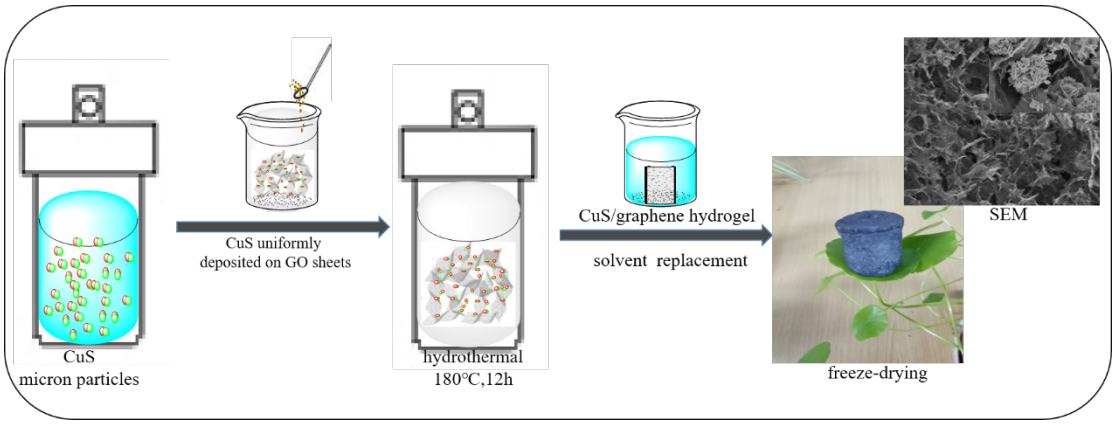

Fig. 1. Schematic illustration of the synthetic process of 3D-CuS/RGO composite.

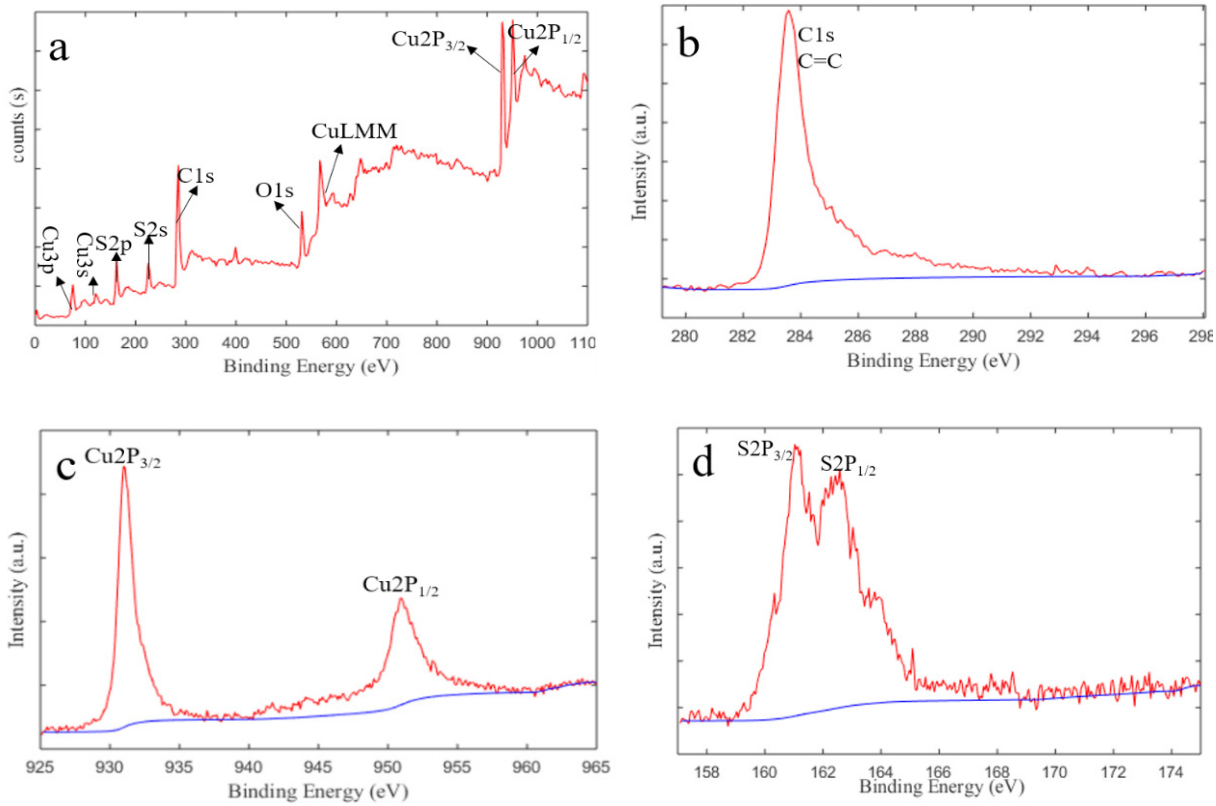

Fig. 2. (a) Wides can XPS survey and high resolution XPS spectrum, (b) C1s, (c) Cu2p, (d) S2p.

2.5. Characterization

The samples' XPS was characterized on a Physical Electronics 5400 ESCA.PANalyticalX'Pert Pro X-ray diffractometer was used to test the XRD spectra by applying the CuKα (λ = 1.54 Å) irradiation at the 2θ range of 10°–80°. Raman spectra were characterized on a Horiba Jobin-Yvon Lab RAM HR800 with a 350 nm irradiation. SEM was used to investigate the sample morphologies and micro sizes at an acceleration voltage of 25 kV. UV-Vis absorption spectra were measured for the performance of optical on a Shimadzu UV-2550 spectrophotometer.

3. Results and discussion

3.1.1. XPS analysis

The compositions of samples were characterized by XPS analysis. From Fig. 2, the wide scan XPS spectra clearly indicated the obtained sample is composed of Cu, S, C, and O. As shown in Fig. 2b, the C=C of graphene was characterized by the strong peak at 284.3 eV in spectrum of carbon [17]. Fig. 2c shows the spectrum of Cu 2p region. The binding energy of Cu $2p_{3/2}$ and Cu $2p_{1/2}$ were investigated by peaks at 932.2 and 952.1 eV respectively, which were highly

corresponded to the values of Cu^{2+} [18,19]. Fig. 2d shows the XPS spectrum of S2p, the binding energy of $S2p_{3/2}$ and $S2p_{1/2}$ were characterized by peaks at 161.6 and 162.8 eV, respectively [20]. In conclusion, all the XPS data and similar values for the binding energy and kinetic energy of Auger electrons demonstrated that the CuS/graphene was successfully prepared [21].

3.1.2. XRD analysis

XRD analysis was used to investigate the crystal forms and purity of the as-prepared CuS and CuS/graphene. From Fig. 3, XRD pattern for CuS exhibited several sharp diffraction peaks at 2θ = 27.8991, 29.5761, 31.7831, 33.1961, 39.2991, 47.9301 and 52.7971, corresponding to the (101), (102), (103), (006), (110), (108) and (116) crystal planes of CuS, respectively, matching well with the hexagonal phase of CuS (JCPDS no. 00-006-0464). Since the diffraction peaks of pure CuS matched well with the sharp and narrow peaks of CuS/graphene, CuS was justified to be a significant component of CuS/graphene. Moreover, the absence of other relevant characteristic peaks (corresponding to impurities) indicates a high purity of the as-prepared CuS/graphene [22].

3.1.3. FTIR spectra analysis

Fig. 4 shows FTIR spectrum, obviously, the FTIR spectrum of GO exhibited several characteristic peaks of oxygen-containing functional groups, i.e., the wide peak at 3450 cm^{-1} belonged to O–H; the peaks at 1730 cm^{-1} and 1392 cm^{-1} belonged to characteristic stretching vibrations of carboxyl –C=O and -C-O respectively. The epoxy C-O stretching was also observed at 1209 cm^{-1} [23]. However, the intensities of all characteristic absorption peaks in spectrum of CuS/GAs were reduced. In particular, the suppression of C=O peak (at 1730 cm^{-1}) indicated an efficient reduction of oxygen-containing functional groups by thiourea [24]. Nevertheless, partial epoxy and hydroxyl groups were retained in CuS/graphene. The FTIR results are also confirmed by the following Raman spectra of CuS/graphene composites.

3.1.4. Raman spectra analysis

Fig. 5 shows a sharp absorption peak at 465 cm^{-1} owing to the vibration of the crystal lattice of CuS [25]. Moreover, the peak of CuS/graphene at 465 cm^{-1} was highly corresponded with that of bare CuS, indicating the introduction of graphene has not affected the structure of CuS. Meanwhile, the Raman spectra also clearly exhibited the characteristics of graphene in the CuS/graphene aerogels. Raman spectra could be used to characterize varies between single-layer graphene, double-layer graphene and graphite [26]. The three most important characteristic peaks of graphene are D, G, and 2D peaks. As Fig. 4 shows, the D peak near 1350 cm^{-1} corresponded to the vibration of sp^3-bonded carbon atoms in disorder or defect sites, and the G band near 1580 cm^{-1} provided information on the in-plane vibration of the sp^2-bonded carbon atoms [27]. The 2D peaks of 2705 cm^{-1} were originated from two-phonon inelastic scattering [28], which was used to distinguish the graphene from graphite. The intensity of the 2D peak of CuS/graphene composite was higher than that of GO, suggesting the reduction process of GO made the interlayer spacing larger [29]. Gener-

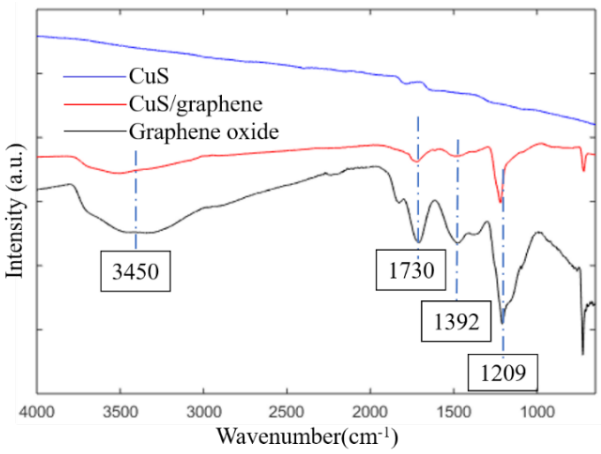

Fig. 4. FTIR spectrum of the obtained pure CuS, graphene oxide and CuS/graphene composites.

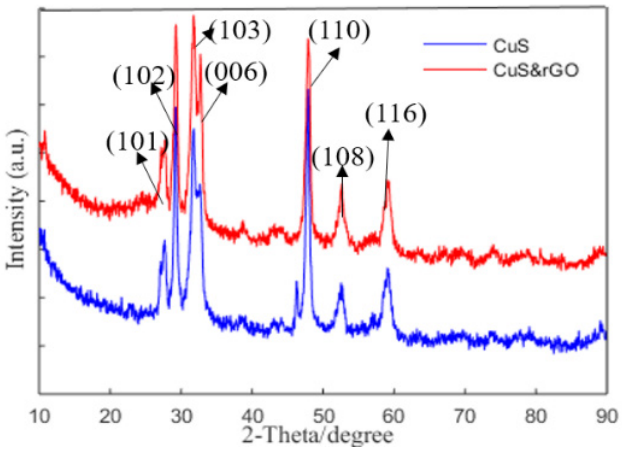

Fig. 3. XRD patterns of the obtained pure CuS and CuS/graphene composites.

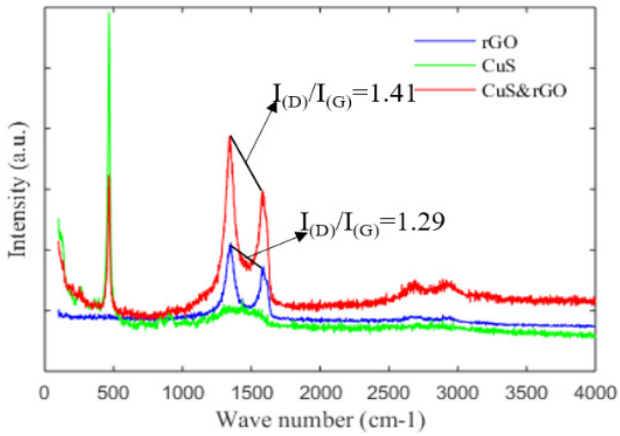

Fig. 5. Raman spectra of the obtained graphene, pure CuS and CuS/graphene composites.

ally, the intensity ratio of the D and G peaks $I_{(D)}/I_{(G)}$ could was investigated the disordered degree and defect density of graphene. It was obvious that the $I_{(D)}/I_{(G)}$ = 1.41 of CuS/graphene composite was higher than that of GO ($I_{(D)}/I_{(G)}$ = 1.29), indicating that the defect density and disordered degree were reduced significantly [30]. Last but not the least, it was obvious that the intensities of D and G peaks increase after introduction CuS into graphene, suggesting that the CuS had a weak Raman enhancement effect [31].

3.1.5. Structure and morphology of the CuS/graphene composite

The SEM images of morphology and microstructure of the CuS/graphene composite are shown in Fig. 6. There were several observations. First, as shown in Fig. 6a, the graphene basement had an interconnected 3D porous structure with pore diameters ranging from several nanometers to several micrometers, which mainly caused by the hydrophobic interaction, π-π conjugation and the intermolecular forces between the graphene sheets after reduction [32]. In the well-constructed micro-, meso- and macroporous 3D network structure, the micro- and mesoporosity provide a high surface area while the macroporosity guarantees the accessibility to the CuSsurface [33]. Second, it is clearly observed from Fig. 6b that hierarchical CuS microspheres are distributed evenly on the 3D porous graphene basement, and it was considered that graphene also had enhanced dispersion of CuS. It was important that the close combination of graphene and CuS also improved the photogenerated charge transfer between CuS and graphene sheets. Furthermore, as shown in Fig. 6c, the CuS microspheres were sandwiched between graphene layers, which would increase graphene layers distance as well as avoid irreversible aggregation of graphene sheets. The increased graphene layers distance guaranteed more space for dye molecules absorbing, thus improved the synergies of adsorption and photocatalysis. Finally, Fig. 6d shows that the flower-like CuS with diameters range from 1 μm to 5 μm were assembled by nanosheets with a thickness of about 50 nm. The hierarchical structures of CuS was beneficial for light reflection and refraction, resulting in the efficiency of utilizing visible-light.

3.1.6. UV-Vis absorption spectra analysis

As an important feature in quantifying the photocatalytic process, the UV–vis absorption spectra of as-obtained pure CuS and CuS/graphene aerogels are shown in Fig. 7a. As can be seen,the pure CuS exhibited a broad absorption band at 550–800 nm, reaching peak at 705 nm. Interestingly, the absorption intensity of CuS/graphene aerogels increased in the whole spectrum due to the absorption contribution of graphene. This was because the introduction of CuS to 3D graphene porous network system could bridge the gap between the incident light and CuS, triggering a photocat-

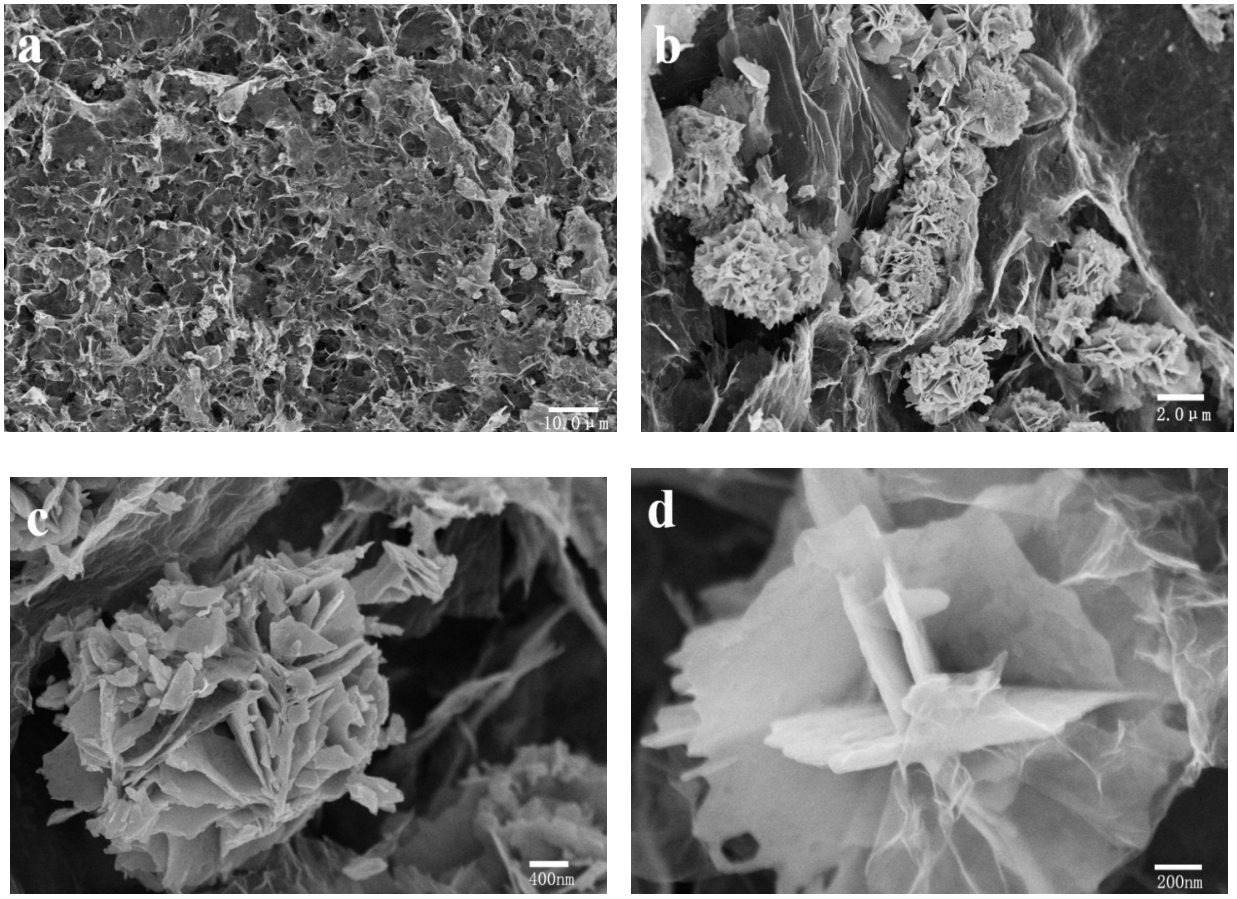

Fig. 6. SEM images of the CuS/graphene composite.

alytic process positively [15]. Remarkably, the optical band gap of the samples was calculated by the relation: $Eg = \frac{hc}{\lambda}$, where c is the speed of light, h is the Planks constant and λ is the wavelength estimated from absorption tail. According to the formula, the bandgap energy of the as-obtained CuS and CuS/graphene composites were 1.35 eV and 1.24 eV, respectively (Fig. 7b). The narrower band gap was caused by the high electronic conduction and migration rate between CuS and graphene, which could enhance the performance of photocatalysis [14]. The CuS/graphene composites with narrower band gap broaden the photo-absorption region and improved photo-quantum efficiency [16]. Consequently, the CuS/graphene composites with the higher light absorbance and the narrower band gap may possess higher photocatalytic degradation efficiency for contaminants in comparison with bare CuS.

3.2. Adsorption and photocatalytic activity of the 3D-3D CuS-RGO composite

MO (50 mg·L^{-1}, pH = 7.0) was chosen to investigate the adsorption capacity of CuS / graphene hydrogels towards anionic dyes. The magnetic stirring and the chopped hydrogel pieces were applied to accelerate the diffusion of adsorbate molecules during the process of the whole adsorption. Fig. 8a shows the adsorption properties of MO by CuS/graphene hydrogels in dark. It was apparent that the removal efficiency of MO increased as the reaction time increased and reached saturation level at 60 min for the CuS/graphene aerogels (at 10 min for pure CuS). 0.1 g of pure CuS could adsorb only about 13.06% of MO, while 0.1 g of the CuS/graphene aerogels could adsorb 36.07% of MO. The data suggested the adsorption capacity of CuS/graphene aerogels was about 2.8 times of the pure CuS, which was attributed to the huge specific surface area and more exposed active sites of 3D network graphene structure. The increased adsorption capacity was in favor of the enrichment of MO from the bulk solution onto the surface of CuS. As a result, the effective reaction of the adsorbed MO to the photogenerated active species on the surface of CuS/graphene composites improved the photocatalytic activity.

As is well known, the photocatalysis of nano-materials was limited by their low adsorption capacity and rapid recombination of the electron-hole pairs. Thus, the novel CuS/graphene porous photocatalyst was prepared for this purpose. The photocatalytic experiments were conducted in the presence of CuS/graphene porous hydrogels under

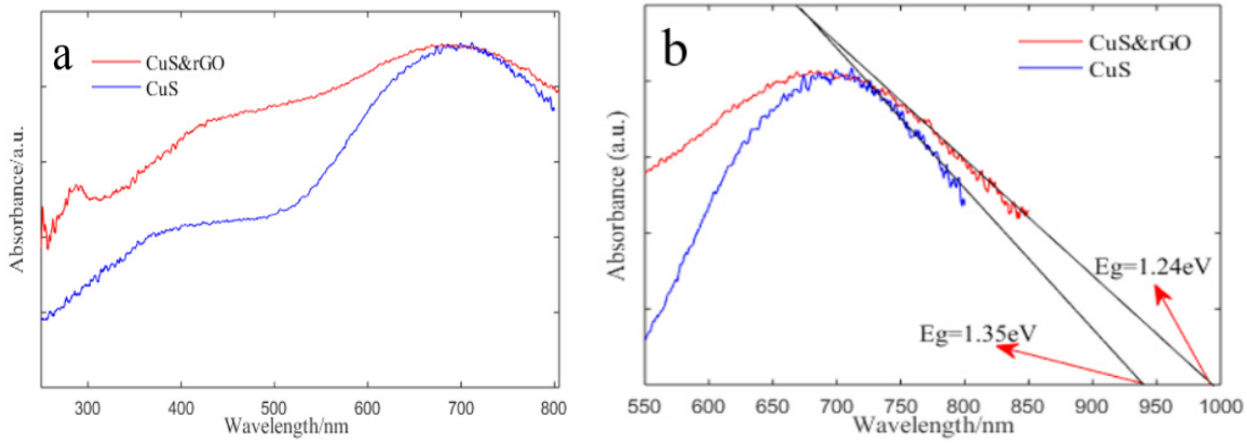

Fig. 7. (a) UV–vis absorption spectra (b) and Band gap spectra of CuS and CuS/graphene hydrogel composites.

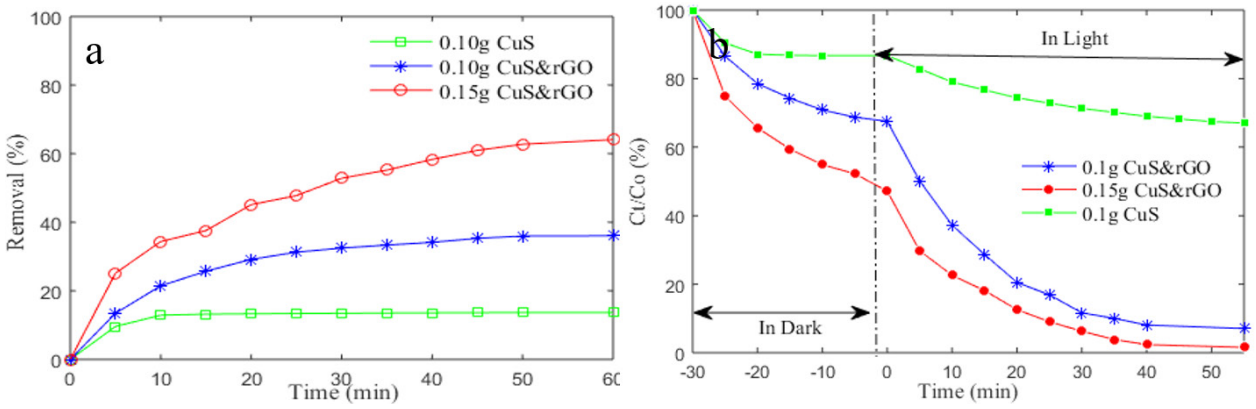

Fig. 8. (a) The adsorption efficiency and (b) the photocatalytic degradation of MO by different samples.

Xenon lamp without assistance of H_2O_2. Firstly, 0.1 g of pure CuS and CuS/graphene were respectively added to the MO solution in the dark condition for 30 min. As Fig. 8b shows the adsorption and desorption on the porous photocatalyst had already been balanced after stirring for 30 min. Remarkably, after irradiation for 55 min under Xenon lamp, the photodegradation rate of bare CuS for MO was only about 32%, while that of CuS/graphene composites went up to as high as 92.94%. The photodegradation efficiency of CuS/graphene was 2.9 times higher than that of bare CuS, indicating the enhancement of photocatalysis efficiency of graphene for MO. This improved photodegradation rate was attributed to the high adsorption capacity and high charge mobility of the 3D porous graphene substrate. Compared to other published CuS composites [14,15], the as-obtained CuS/graphene porous photocatalysts presented excellent removal efficiency for dye wastewater even without the assistance of H_2O_2. Obviously, the introduced graphene played a positive role in the photodegradation and adsorption of dyes. In addition, the CuS/graphene composites of different mass added to MO solution was investigated for photodegradation of MO. Obviously, the degradation of MO climbed from 92% to 99% after illumination for 55 min when the contents of CuS/graphene composites increased from 0.1 to 0.15 g (Fig. 8b). Therefore, in a certain mass range, the photodegradation rate were positive proportional to the mass of photocatalyst.

Fig. 9a shows the UV-Vis absorption spectrum of MO solution treated with 0.1 g of CuS/graphene hydrogels under Xenon lamp at different time. It was easy to see from the spectra, the absorbance of MO at 464 nm decreased slowly in the initial 30 min of dark reaction, while then had a sharp decline with condition of Xenon lamp irradiation. After illumination for 55 min, MO had been thoroughly degraded, suggesting the photocatalysis of CuS/graphene composites for MO had achieved the expected effect. Thus, the synergism of photocatalysis and adsorption has proven to be an effective means for wastewater treatment compared to adsorption only, owing to the rapid photodegradation of contaminants adsorbed on the photocatalyst surface [34]. The kinetic curve was applied to explain degradation behavior of CuS/graphene composites. The corresponding scatter plot of experimental results shown in Fig. 9b agree well with the solid line calculated according to the pseudo-first-order kinetics model. Therefore, the MO degradation efficiency of synergistic of adsorption and photocatalysis increased with the content increase of CuS/graphene composites. Finally, the concentration of MO solution was also an important factor which affected the photodegradation rate of MO. As shown in Fig. 9b, the photocatalytic rate constant increased with the increase of the solution concentration.

In order to further understand the dye degradation efficiency loss, the BET surface area values of the CuS/graphene photocatalyst before absorption and after photodegradation were characterized by the nitrogen isotherm absorption-desorption measurement. As can be seen from Fig. 10, the N_2 adsorption-desorption isotherms of before absorption and after photodegradation belong to the IV hysteresis loop according to IUPAC. The specific surface areas of CuS/graphene before absorption was calculated to be 114.5 $m^2 \cdot g^{-1}$. And the values of the catalyst after photo-

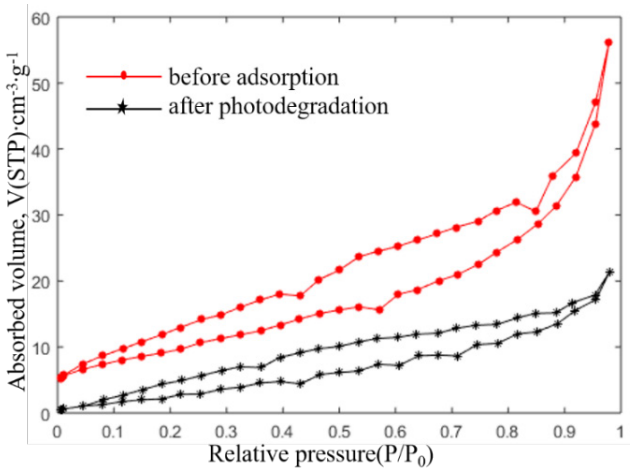

Fig. 10. N_2 adsorption–desorption Isotherms of the CuS/graphene photocatalyst.

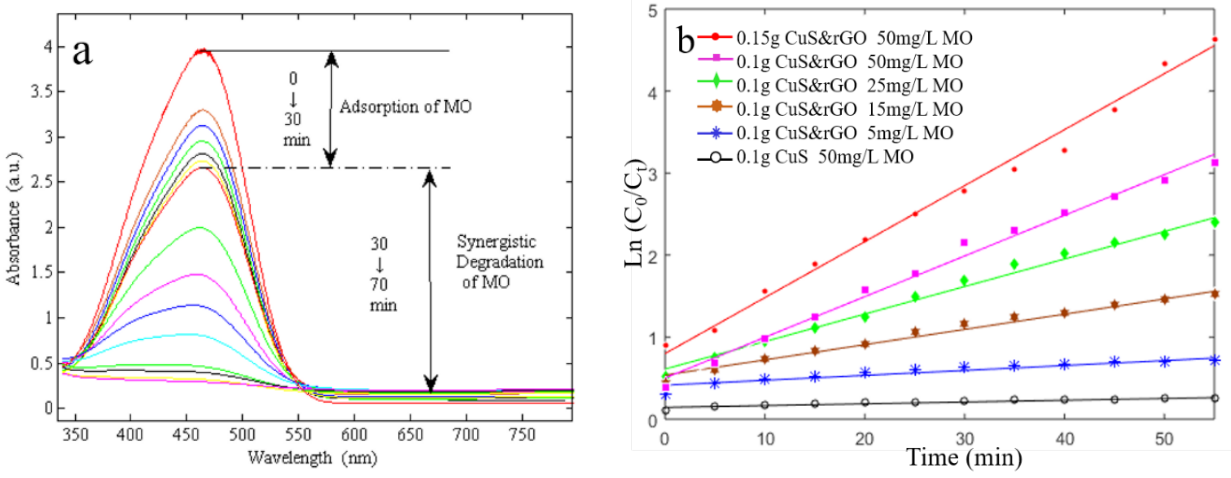

Fig . 9. (a) Time-dependent photodegradation spectrum of MO in the presence of 0.1 g CuS/graphene samples; (b) Pseudo first-order photo-degradation kinetics of MO with 0.1 g CuS, 0.1 and 0.15 g of CuS/graphene.

degradation drop to 78.5 $m^2 \cdot g^{-1}$, which was 1.46 times less than that of the photocatalyst before absorption. The larger surface areas before absorption may be the main reason for the decrease of dye concentration in the dark. After photocatalysis, the specific surface area of the CuS/graphene composites decreased greatly, which may be caused by the adsorption-enriched dye blocking a large number of nano-sized micropore in the 3D graphene network. Finally, experimental operations such as magnetic stirring, centrifugation, and vacuum freeze-drying will cause some macropores and mesopores in the CuS/graphene composite to collapse, which is also an important reason for the sharp decrease of specific surface area.

Fig. 11 shows the FTIR spectra of CuS/graphene, methyl orange, CuS/graphene after adsorption and CuS/graphene after photodegradation. The FTIR spectrum analysis of the CuS/graphene (Fig. 11a) was referred to earlier in this article. As shown in the methyl orange (Fig. 11b), 1620 cm^{-1} and 1520~1450 cm^{-1} were attributed to the benzene skeleton vibration and the vibration of C=C on the benzene ring. 835 cm^{-1} was the vibration of the substituent in p-position on the benzene ring. The peaks at 1450 cm^{-1} and 1370 cm^{-1} were the stretching vibration peak of N=N and C-N, respectively. In addition, 1228 cm^{-1}, 1028 cm^{-1}, 1007 cm^{-1}, 620 cm^{-1} and 530 cm^{-1} were the main characteristic peaks of the sulfonic group. As for the CuS/graphene after adsorption of MO (Fig. 11c), the peaks at 1620~530 cm^{-1} were highly similar to methyl orange, which indicated that the graphene network was an excellent substrate for adsorbing MO. It was noteworthy that the broad and strong peak at 3450 cm^{-1} was attributed to the vibration of hydroxyl groups or/and adsorbed water molecules on the surface of the sample. Compared with Fig. 11c, the N=N (1450 cm^{-1}) and C-N (1370 cm^{-1}) peaks of the CuS/graphene after photodegradation (Fig. 11d) were significantly decreased, indicating that the N=N in MO molecules was opened. Meanwhile, the absorption peak intensity of the benzene skeleton vibration (1620 cm^{-1}) and the substituent in p-position on the benzene ring (835 cm^{-1}) become very weak, indicating that many benzene rings of MO molecules were also opened. Finally, the main characteristic peaks' absorption intensity of the sulfonic groups also drastically decreased, indicating that a large amount of the sulfonic acid groups in the MO were catalytically decomposed. In summary, the above analysis further confirmed that the CuS/graphene complex has excellent photocatalytic degradation to methyl orange.

The stability and recyclability of CuS/graphene porous photocatalyst was also an important parameter to estimate the performance of photocatalysis, which was carried out by repeat photodegradation of MO. Fig. 12 shows the cycling stability of CuS/graphene composite, the porous catalyst was washed before the next reaction. In the first cycle, 36.07% of MO was adsorbed by 0.1 g of CuS/graphene porous composite, and lower values of 32.78% and 29.31% were adsorbed in the second and third cycles, respectively. It was easily found that the adsorption ability decreased with the increase number of cycles. Remarkably, the efficiency of adsorption synergistic photocatalytic degradation of MO was far better than the adsorption efficiency. The MO removal efficiency still remained 79.47% in the third cycle, indicating that the CuS/graphene hydrogels resolved the adsorption saturation problem of graphene hydrogel and had a high stability. Therefore, the synergies of adsorption and photocatalysis was proved to be a more efficient measures for dyestuff wastewater treatment compared to the adsorption.

3.2.3. Photocatalytic mechanisms

The following showed a possible photocatalytic mechanism of CuS/graphene. The high dye removal efficiency was mainly associated with effectively inhibiting the recombination of electron-hole pairs and high adsorption capacity. First, the interconnected micro-, meso-, and macrospores provided dye sorption channels which promoted the synergy of dyestuff adsorption-enrichment and photo-catalytic degradation. More specifically, the macropores with high adsorption capacity guaranteed a short diffusion distance to the interior surfaces, while the plentiful micro- and mesopores guarantee high surface area and a large amount oxygen-containing functional group adsorption sites. Moreover, the 3D graphene structure could rapidly accept and transfer photogenerated electrons from the

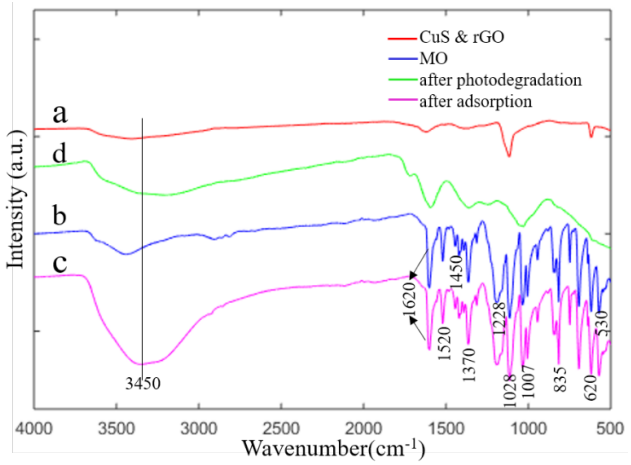

Fig. 11. The FTIR spectra of the photocatalyst before adsorption and after photodegradation.

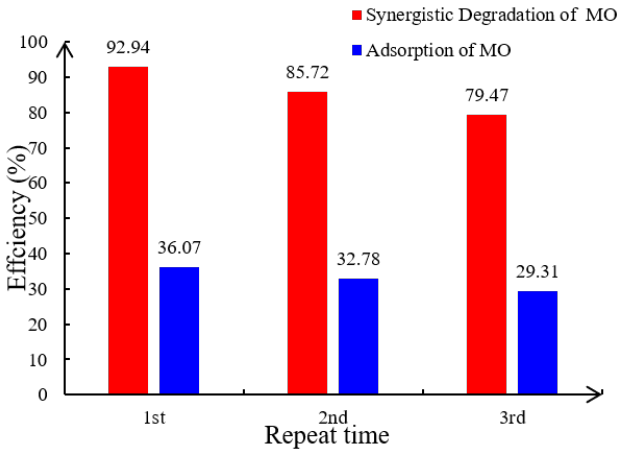

Fig. 12. Cycling stability of CuS/graphene composite under different conditions.

conduction band of CuS. Thus, it could boost the effcient separation of electron-hole pairs, resulting in an excellent photocatalytic activity of CuS/graphene composite aerogels [35]. Meanwhile, the photogenerated electrons would react with adsorbed oxygen to generate O_2·- and holes would react with H_2O to form ·OH. Both the O_2·- and ·OH radicals could completely oxidize contaminants into H_2O and CO_2. Therefore, the CuS/graphene porous composites showed excellent removal efficiency for organic dyestuff in this work.

4. Conclusion

In conclusion, we successfully prepared a novel 3D CuS/graphene porous photocatalyst via two-step solvothermal method. Methyl orange could be adsorbed rapidly by the 3D graphene porous network and then was photodegraded rapidly by flower-like CuS under Xenon lamp irradiation. Due to the outstanding synergy of adsorption and degradation activities, the photodegradation of the CuS/graphene for MO was reached to a value of 92.94% even without the assistance of H_2O_2, which was about 2.9 times higher than that of bare CuS. Finally, cycling stability tests revealed the MO removal efficiency still remained 79.47% after three repeated cycles, indicating that the novel 3D CuS/graphene porous photocatalyst had a high recyclability for degradation of MO. Thus, we have successfully synthesized an efficient and recyclable photocatalyst for removing organic dyestuff and provide a novel route for wastewater treatment.

Acknowledgements

This work was supported by National Natural Science Foundation of China (51703123). This research was also supported by the Talent Program of Shanghai University of Engineering Science and Innovation.

Note: The authors declare no conflict of interest.

References

[1] H. Cong, X. Ren, P. Wang, H. Yu, Macroscopic multifunctional graphene-based hydrogels and aerogels by a metal ion induced self-assembly process, ACS Nano, 6(3) (2012) 2693– 2703.
[2] Y. Lei, F. Chen, Y. Luo, L. Zhang, Three-dimensional magnetic graphene oxide foam/Fe_3O_4, nanocomposite as an efficient absorbent for Cr (VI) removal, J. Mater. Sci., 49(12) (2014) 4236–4245.
[3] R. Xu, G. Zhou, Y. Tang, L. Chu, C. Liu, Z. Zeng, S. Luo, New double network hydrogel adsorbent: Highly efficient removal of Cd (II) and Mn (II) ions in aqueous solution, Chem. Eng. J., 275 (2015) 179–188.
[4] M. Ge, C. Cao, J. Huang, S. Li, Z. Chen, K. Zhang, S. Al-Salem, Y. Lai, A review of one-dimensional TiO_2 nanostructured materials for environmental and energy applications, J. Mater. Chem. A, 4(18) (2016) 6772–6801.
[5] G. Sharma, A. Kumar, M. Naushad, D. Pathania, M. Sillanpää, Polyacrylamide (IV) @ Zr (II) vanadophosphate nanocomposite: Ion exchange properties, antibacterial activity, and photocatalytic behavior, J. Ind. Eng. Chem., 33 (2016) 201–208.
[6] D. Pathania, R. Katwal, G. Sharma, M. Naushad, M. Rizwan Khan, A. Al-Muhtaseb, Novel guar gum/ Al_2O_3 nanocomposite as an effective photocatalyst for the degradation of malachite green dye, Int. J. Biol. Macromol., 87 (2016) 366–374.
[7] F. Chen, W. An, L. Liu, Y. Liang, W. Cui, Highly efficient removal of bisphenol A by a three-dimensional graphene hydrogel-AgBr@rGO exhibiting adsorption/photocatalysis synergy, Appl. Catal. B Environ., 217 (2017) 65–80.
[8] W. Lü, J. Chen, Y. Wu, L. Duan, Y. Yang, X. Ge, Graphene-enhanced visible-light photocatalysis of large-sized CdS particles for wastewater treatment, Nanoscale Res. Lett., 9(1) (2014) 148.
[9] Y. Li, H. Zhang, P. Liu, D. Wang, Y. Li, H. Zhao, Cross-linked g-C_3N_4/rGO nanocomposites with tunable band structure and enhanced visible light photocatalytic activity, Small, 9(19) (2013) 3336–3344.
[10] Y. Li, W. Cui, L. Liu, R. Zong, W. Yao, Y. Liang, Y. Zhu, Removal of Cr (VI) by 3D TiO_2- graphene hydrogel via adsorption enriched with photocatalytic reduction, Appl. Catal. B Environ., 199 (2016) 412–423.
[11] G.C. Yadav, G. Sharma, S. Kumar, V. Singh, Performance study of metallic clad planar waveguide sensors in presence of graphene layer, Optik– Int. J. Light Electron Optics, 147 (2017) 366–372.
[12] Z. Nan, M.Q. Yang, S. Liu, Y. Sun, Y. Xu, Waltzing with the versatile platform of graphene to synthesize composite photocatalysts, Chem. Rev., 115(18) (2015) 10307–10377.
[13] W. Jiang, Y. Zhu, G. Zhu, Z. Zhang, X. Chen, W. Yao, Three-dimensional photocatalysts with network structure, J. Mater. Chem. A, 5(12) (2017) 5661–5679.
[14] J. Yu, J. Zhang, S. Liu, Ion-exchange synthesis and enhanced visible-light photoactivity of CuS/ZnS nanocomposite hollow spheres, J. Phys. Chem. C, 114(32) (2010) 13642–13649.
[15] S.B. Aziz, R.T. Abdulwahid, H.A. Rsaul, H.M. Ahmed, In situ synthesis of CuS nanoparticle with a distinguishable SPR peak in NIR region, J. Mater. Sci. Mater. Electron., 27(5) (2016) 4163–4171.
[16] W.S. Hummers, R.E. Offeman, Preparation of graphitic oxide, J. Am. Chem. Soc., 80(6) (1958) 1339.
[17] S.W. Lee, C. Mattevi, M. Chhowalla, R.M. Sankaran, Plasma-assisted reduction of graphene oxide at low temperature and atmospheric pressure for flexible conductor applications, J. Phys. Chem. Lett., 3(6) (2012) 772–777.
[18] J. Qian, K. Wang, Q. Guan, H. Li, H. Xu, Q. Liu, W. Liu, B. Qiu, Enhanced wet hydrogen peroxide catalytic oxidation performances based on CuS nanocrystals/reduced graphene oxide composites, Appl. Surf. Sci., 288 (2014) 633–640.
[19] Q.W. Shu, J. Lan, M.X. Gao, J. Wang, C.Z. Huang, Controlled synthesis of CuS caved superstructures and their application to the catalysis of organic dye degradation in the absence of light, Cryst. Eng. Comm., 17 (2015) 1374–1380.
[20] L.L. Li, P.N. Zhu, S.J. Peng, M. Srinivasan, Q.Y. Yan, A.S. Nair, B. Liu, S. Samakrishna, Controlled growth of CuS on electrospun carbon nanofibers as an efficient counter electrode for quantum dot-sensitized solar cells, J. Phys. Chem. C, 118 (2014) 16526–16535.
[21] J. Shi, X. Zhou, Y. Liu, Q. Su, J. Zhang, G. Du, Sonochemical synthesis of CuS/reduced graphene oxide nanocomposites with enhanced absorption and photocatalytic performance, Mater. Lett., 126 (2014) 220–223.
[22] S. Dutta, C. Ray, S. Mallick, S. Sarkar, R. Sahoo, Y. Negishi, T. Pal, Synthesis of a flower-like CuS/ZnS nanocomposite decorated on reduced graphene oxide and its photocatalytic performance, RSC Adv., 5 (2015) 36185–36191.
[23] P. Liu, Y. Huang, J. Yan, Y. Yang, Y Zhao, Construction of CuS nanoflakes vertically aligned on magnetically decorated graphene and their enhanced microwave absorption properties, ACS Appl. Mater. Interf., 8(8) (2016) 5536–5546.
[24] L. Yang, X. Guan, G.S. Wang, X. Guan, B. Jia, Synthesis of ZnS/CuS nanospheres loaded on reduced graphene oxide as high-performance photocatalysts under simulated sunlight irradiation, New J. Chem., 41(13) (2017) 5732–5744.

[25] K.R. Nemade, S.A. Waghuley, Band gap engineering of CuS nanoparticles for artificial photosynthesis, Mat. Sci. Semicon. Proc., 39 (2015) 781–785.
[26] X. Chen, Q. Chen, W. Jiang, Z. Wei, Y. Zhu, Separation-free TiO_2-graphene hydrogel with 3D network structure for efficient photo-electrocatalytic mineralization, Appl. Catal. B Environ., 211 (2017) 106–113.
[27] Y. Sun, Q. Wu, G. Shi, Graphene based new energy materials, Energy Environ. Sci., 4(4) (2011) 1113–1132.
[28] A.C. Ferrari, J. Meyer, V. Scardaci, C. Casiraghi, M. Lazzeri, F. Mauri, S. Piscanec, D. Jiang, K.S. Novoselov, S. Roth, A.K. Geim, Raman spectrum of graphene and graphene layers, Phys. Rev. Lett., 97(18) (2006) 187401–187405.
[29] N. Lamaison, C.L. Ong, J.B. Marcinichen, J.R. Thome, Two-phase mini-thermosyphon electronics cooling: dynamic modeling, experimental validation and application to 2U servers, Appl. Thermal Eng., 110 (2016) 481–494.
[30] A. Kaniyoor, T.T. Baby, T. Arockiadoss, N. Rajalakshmi, S. Ramaprabhu, Wrinkled graphenes: a study on the effects of synthesis parameters on exfoliation-reduction of graphite oxide, J. Phys. Chem. C, 115(36) (2011) 17660–17669.
[31] H. Zhao, S.U. Fang, X. Fan, H. Yu, D. Wu, X. Quan, Graphene-TiO_2 composite photocatalyst with enhanced photocatalytic performance, Chinese J. Catal., 33(4–6) (2012) 777–782.
[32] Y. Fan, W. Ma, D. Han, S. Gan, X. Dong, L. Niu, Convenient recycling of 3D AgX/graphene aerogels (X = Br, Cl) for efficient photocatalytic degradation of water pollutants, Adv. Mater., 27 (2015) 3767–3773.
[33] C. Ding, D. Su, W. Ma, Y. Zhao, D. Yan, J. Li, H. Jin, Design of hierarchical CuS/ graphene architectures with enhanced lithium storage capability, Appl. Surf. Sci., 403 (2017) 1–8.
[34] C. Xiong, X. Deng, J. Li, Preparation and photodegradation activity of high aspect ratio rutile TiO_2, single crystal nanorods, Appl. Catal. B Environ., 94(3–4) (2010) 234–240.
[35] Y. Hou, F. Zuo, A.P. Dagg, J. Liu, P. Feng, Branched WO3 nanosheet array with layered C_3N_4 heterojunctions and CoOx nanoparticles as a flexible photoanode for efficient photoelectrochemical water oxidation, Adv. Mater., 26(29) (2014) 5043–5049.